



Research on the Wear of Groove Structured Grinding Wheel Based on the Simulation and Experiment of Single Abrasive Particle Scratching

Jun Yi^{1,2} · Zongwei Wang² · Tao Yi² · Hui Deng^{1,2} · Wei Zhou^{1,2}

Received: 28 October 2023 / Revised: 1 February 2024 / Accepted: 2 February 2024 / Published online: 4 March 2024
© The Author(s), under exclusive licence to Korean Society for Precision Engineering 2024

Abstract

In order to comprehend the abrasive wear mechanism of CBN grinding wheels with varying structural characteristic parameters, the influence of these parameters on abrasive wear was transformed into the impact of undeformed chip thickness on abrasive wear. Subsequently, a two-dimensional finite element simulation model of single CBN abrasive scratching was established. The effects of different maximum undeformed chip thicknesses, scratching speeds, and abrasive rake angles on wear morphology and normal scratching force were analyzed. Furthermore, the simulation model was validated through single abrasive scratching experiments. The results indicate that the predominant form of CBN particle wear is crushing and fracture. During the scratching process, wear consistently initiates with micro-crushing and micro-cracks between the particle tip and front tool face. As this process continues, cracks propagate within the particle until ultimately causing its fracture. When holding constant both scratching speed and abrasive rake angle, an increase in maximum undeformed chip thickness (i.e., intermittent ratio of grinding wheel) leads to elevated normal scratching force and greater degree of abrasive wear. Moreover, an increase in scratching speed exacerbates abrasion while an increase in abrasive rake angle reduces scratching force thereby alleviating the abrasion process.

Keywords Structured grinding wheel · Grinding wheel wear · Single CBN abrasive scratching

1 Introduction

The major issue during the grinding process with structured grinding wheels is the severe abrasive wear on the surface of the wheel [1]. Abrasive wear occurs when abrasive particles and workpiece materials experience high temperature and stress, resulting in the removal of abrasive material due to friction [2]. The shape, arrangement of abrasives, grinding process parameters, and wheel structure all have an impact on abrasive wear. Understanding the laws of abrasive wear evolution and the influence of various factors on it is essential for rational planning of grinding parameters,

optimization of grinding wheel design, and prolonging the service life of grinding wheels.

Finite element analysis can efficiently simulate the grinding process of single or multiple abrasive particles, providing a convenient means to comprehend stress and temperature distribution, as well as the formation and wear processes of abrasive chips [3]. Researchers have utilized the finite element method to conduct a series of studies analyzing abrasive wear.

Jackson [4] employed the finite element method to simulate the fracture and wear process of CBN grinding wheels. The simulation results showed that abrasive crushing is mainly responsible for abrasion failure on their surfaces due to mechanical tensile stresses within abrasives surpassing compressive ones. Additionally, it had been discovered that a correlation exists between pull force and grinding ratio in these wheels. Su et al. [5] proposed a smoothed particle hydrodynamics (SPH) method for simulating the cutting process of a single CBN particle, with the aim of addressing mesh constraints inherent in traditional finite element methods used to simulate such processes. Through observation of

✉ Jun Yi
yj_hnust@163.com

¹ Hunan Provincial Key Laboratory of High Efficiency and Precision Machining of Difficult-to-Cut Material, Hunan University of Science and Technology, Xiangtan 411201, China

² College of Mechanic Engineering, Hunan University of Science and Technology, Xiangtan 411201, China

changes in stress fields and movement of smooth particles on its surface during simulation, they analyzed the crushing and chip deformation mechanisms of the CBN particle. The results indicate that the front cutter surface of abrasive particles is prone to micro-crushing and wear platforms due to stress concentration, while the workpiece is propelled forward by the abrasive particles, resulting in chip formation. Zhang [6] utilized the random section method to construct an irregular single CBN particle and conducted simulations of its scraping on 45 steel and 40CrNiMoA steel using the smooth particle hydrodynamic method. The simulation model was validated through an orthogonal test, and the wear morphology of the simulated particle corresponded with that observed in experimental results. Ding et al. [7] conducted high-speed grinding experiments on single wear particles of cubic boron nitride and polycrystalline cubic boron nitride, respectively. The wear behavior of the two wear particles was compared based on fractal analysis. It was observed that the wear behavior of single crystal cubic boron nitride generally adheres to the periodic pattern of micro-wear, macro-crushing, micro-crushing and wear. On the other hand, polycrystalline cubic boron nitride exhibits a periodic trend of micro-fracture, wear and micro-fracture. Additionally, polycrystalline cubic boron nitride particles possess higher fractal dimension which indicates superior self-sharpening ability and wear resistance. Ding [8] utilized Abaqus software to simulate the stress resulting from brazing and grinding during the grinding process of a single brazed CBN particle, and subsequently compared the stress distribution of said particle under six varying degrees of wear. As the wear conditions deteriorate, the combined stresses of brazing and grinding have a reduced impact on the bottom of the wear particle, with most of it concentrated at its apex. The combined stress is primarily concentrated at the apex of the wear particle, leading to micro-crushing, while macro-crushing is caused by high tensile stress at the junction between the wear particle and matrix. Mei et al. [9] proposed a method that utilizes finite element software to simulate the wear evolution process of particles. Initially, the stress distribution within a single particle was obtained through a two-dimensional scratch simulation, and then failed elements were removed based on the failure strength and stress distribution. Finally, updating the abrasion morphology by removing the failed element allowed for completion of the scratch simulation in subsequent steps. Repeating this process provided valuable insight into the evolution of abrasive wear. The simulation results indicate that the grinding force exhibits fluctuations in response to changes in the number of cutting edges, owing to a dynamic process of wear and self-sharpening experienced by abrasive particles. Furthermore, an increase in the number of cutting edges leads to a reduction in chip volume due to enhanced ploughing action exerted by abrasive particles during wear.

Wang et al. [10] (based on Mei's method) conducted further simulations using Abaqus to investigate the wear process of a single CBN abrasive particle scraping against high-temperature nickel-based alloy 718. The numerical evaluation of the abrasive particle's wear was based on its tensile strength and hardness, revealing that the wear behavior of the CBN abrasive particle could be categorized into two distinct forms. One is the macroscopic fracture occurring on the top surface of the abrasive grain, and the other is the microscopic fracture happening at the edge of the abrasive cutting edge. Rao [11] proposed a two-dimensional finite element model to simulate the fracture and wear behavior of polycrystalline CBN particles during high-speed scratching. A geometric model of polycrystalline CBN particles was constructed using the Tyson polygon, and a cohesive element was added to simulate the crack propagation process in the model. The influence of cohesive chip thickness on the wear of CBN particles was analyzed in detail. The results indicate that abrasive wear primarily occurs in the vertex region of abrasive particles, while the fracture behavior of abrasive particles mainly takes place near the grain boundary. Abrasive particles are more likely to break when the thickness of undeformed chips exceeds 1 μm . Wang [12] combined the methods of Mei and Rao to conduct a simulation study on the process of wear evolution in polycrystalline CBN particles. The results indicate that the fracture modes of polycrystalline CBN wear particles primarily consist of cutting edge breakage due to stress concentration and crack propagation caused by non-uniform deformation. The tensile force is the main factor affecting the fracture of wear particles and the breaking of wear particles leads to a dynamic cycle of passivation-sharpening. Bergs [13] studied the fracture behavior of abrasive grains in the dressing process of CBN grinding wheel by finite element method, and analyzed the influences of abrasive grain shape, dressing parameters, abrasive protrusion height and abrasive grain orientation on abrasive grain fracture. The results showed that the shape and orientation of abrasive grains exerted the most significant influence on their fracture. Wang [14] used near field dynamic method to study the fracture mechanism of abrasive grains during grinding with CBN grinding wheel, compared the fracture behavior of three different abrasive grains during dressing, and found that the fracture of abrasive grains generally went through four stages: elastic deformation, damage initiation, crack formation and macro fracture. The initiation and propagation of fracture mainly depend on tensile stress and shear stress, in which tensile stress leads to type I fracture, while shear stress leads to type II fracture.

The above researches mainly focuses on the mechanism of abrasive wear. For structured grinding wheels, different structural characteristics will lead to different forms of abrasive wear. Analyzing the influence of structural characteristics and grinding parameters on abrasive wear is of great

significance for understanding the wear mechanism of grinding wheels and improving the durability of grinding wheels.

2 Analysis of Abrasive Wear on the Surface of Structured Grinding Wheel

Figures 1 and 2 display the wear of grinding wheels with groove widths of 6 mm and intermittent ratios of 1:3.4 and 1:4.2, respectively. It is apparent that the abrasive particles of the grinding wheel with two types of intermittent ratios primarily crush in non-grooved areas, while those adjacent to the grooves fracture to varying degrees. Abrasive particles with severe fractures directly lose their

grinding ability. Upon comparing the wear conditions of grinding wheels with two different intermittent ratios near the groove, it is evident that the wheel with a larger intermittent ratio experiences more severe abrasion. The wear on the structured grinding wheel near the groove consistently exhibits a severe pattern, as evident from the aforementioned results. The wear situation in proximity to the groove of the grinding wheel is closely associated with its structural parameters, primarily due to their influence on the maximum undeformed chip thickness of the grinding wheel. Consequently, this leads to variations in stress levels experienced by abrasive particles during grinding and subsequently gives rise to diverse forms of abrasive particle wear.

Fig. 1 Wear condition of structured electroplated CBN grinding wheel with groove width of 6 mm and intermittent ratio of 1:3.4. **a** Overall photograph of grinding wheel, **b** Partial photograph of grinding wheel, **c** Non grooved areas, **d** Near groove

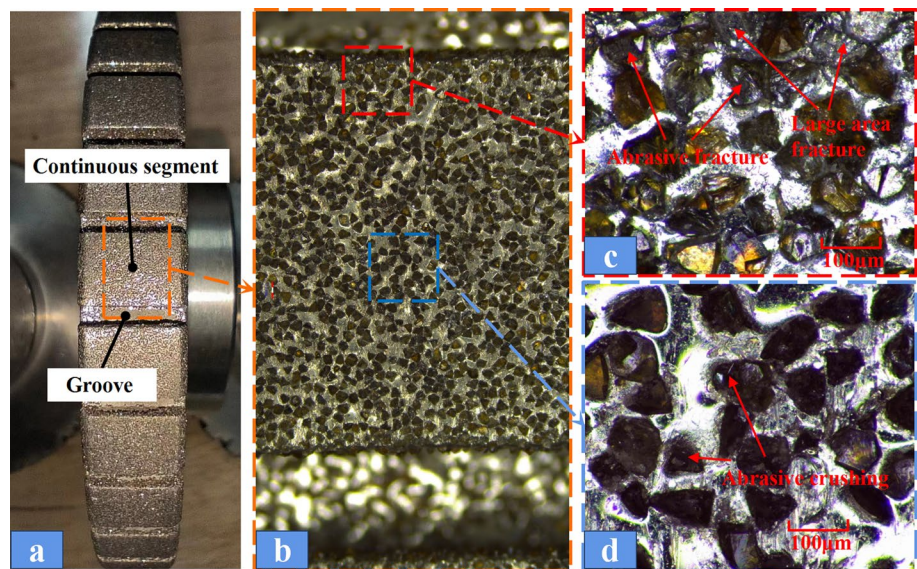
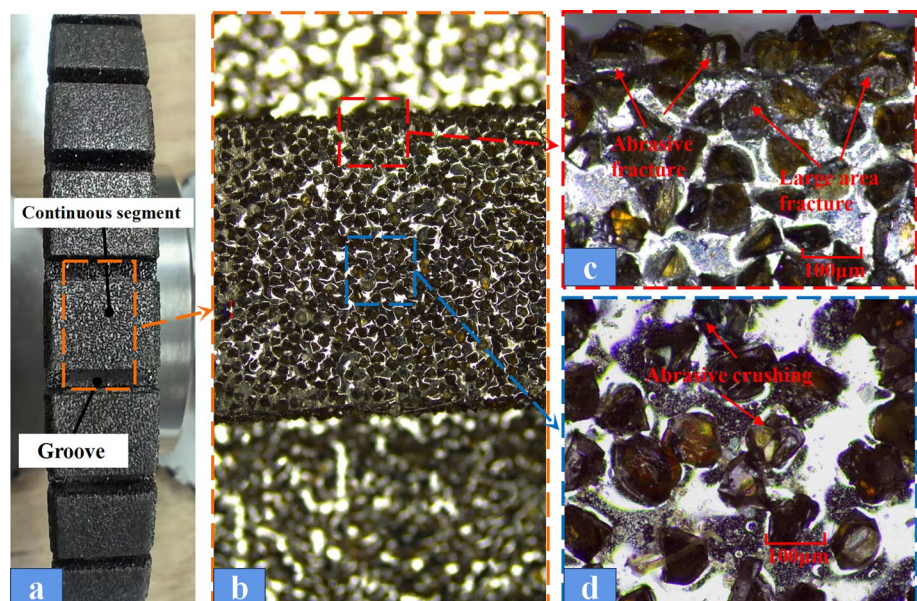


Fig. 2 Wear condition of structured electroplated CBN grinding wheel with groove width of 6 mm and intermittent ratio of 1:4.2. **a** Overall photograph of grinding wheel, **b** Partial photograph of grinding wheel, **c** Non grooved areas, **d** Near groove



In order to investigate the impact of various structural parameters on abrasive wear of grinding wheel surface, it is imperative to first analyze the correlation between these parameters and maximum undeformed chip thickness.

The maximum undeformed chip thickness of a straight grooved structured wheel with groove width (l_g) and continuous arc length of the grinding wheel (l_w) can be mathematically expressed under the given conditions of grinding speed (v_s), workpiece feed speed (v_w), and grinding depth (a_p) as follow [15]

$$a_{g\max} = \sqrt{\frac{4}{rC} \cdot \frac{v_w}{v_s} \cdot \sqrt{\frac{a_p}{D}} \cdot \frac{l_w + l_g}{l_w}} \quad (1)$$

where C represents the dynamic effective number of abrasive particles per unit area, r denotes the width to thickness ratio of abrasive chips, and D stands for the diameter of the grinding wheel.

According to Eq. (1), when the groove width (l_g) remains unchanged, an increase in the intermittent ratio (l_g/l_w) will result in an increase in the maximum undeformed chip thickness. Conversely, when the intermittent ratio (l_g/l_w) is constant, changes in groove width (l_g) will not affect the maximum undeformed chip thickness.

Based on the aforementioned analysis, it becomes evident that variations in the maximum undeformed chip thickness resulting from changes in intermittent ratio are ultimately responsible for the varying degrees of wear observed on structured grinding wheels. Consequently, investigating the impact of structural parameters on abrasive wear can be reframed as an examination of how different maximum undeformed chip thicknesses influence abrasive wear. Considering the influence of grinding speed and abrasive rake angle on abrasive wear, the simulation process primarily focuses on investigating the impact of three parameters—maximum undeformed chip thickness, grinding speed, and abrasive rake angle—on abrasive wear.

3 Finite Element Model of Scratching by a Single Abrasive Particle

3.1 Geometric Model of the Workpiece with Abrasive Particle

The process of material removal from a workpiece by abrasive particles on the surface of a grinding wheel is analogous to cutting processing, involving the elimination of workpiece material through shearing slip caused by extrusion. However, the distinction lies in the fact that abrasive particles lack fixed shapes during grinding, resulting in an uneven distribution of stress fields and higher temperatures generated during the abrasive scratching process. This gives rise to a

complex evolution process of abrasive wear that poses challenges for real-time experimental monitoring. The Abaqus software is widely utilized in various fields, including material processing, metal forming, and the evolution of metallographic structures, making it a prevalent choice for general finite element analysis. Its Explicit solver excels at handling highly nonlinear dynamics problems that are both large and complex. In particular, the abrasive friction workpiece process presents a challenging nonlinear problem characterized by significant material deformation, high strain rates, and material damage. Henceforth, this paper selects Abaqus as the simulation software.

Observation of Figs. 1 and 2 reveals that the majority of CBN particles exhibit complex shapes such as tetrahedrons, hexahedrons, and other polyhedrons, making it challenging to establish an accurate particle model. Therefore, simplification of the particle shape is necessary to some extent. While a three-dimensional simulation model provides clearer visualization of abrasive particle flow, its solution requires high computational capabilities. This paper primarily focuses on discussing normal friction force size and abrasive particle wear patterns through two-dimensional simulations for efficient and accurate acquisition of desired information.

The geometric model of a single abrasive particle and workpiece, as established in this paper, is illustrated in Fig. 3. The abrasive particle is composed of CBN material and takes the form of a triangular shape with a tip radius measuring $2 \mu\text{m}$. The abrasive particle was discretized into triangular mesh, and the element type employed is a three-node plane strain-thermal coupling element with a constant size of $0.25 \mu\text{m}$.

On the other hand, the workpiece is made of 20CrMnTi material. Considering the limited penetration depth of the abrasive particle, which is only a few microns, and the small contact area of the machined surface, the dimensions

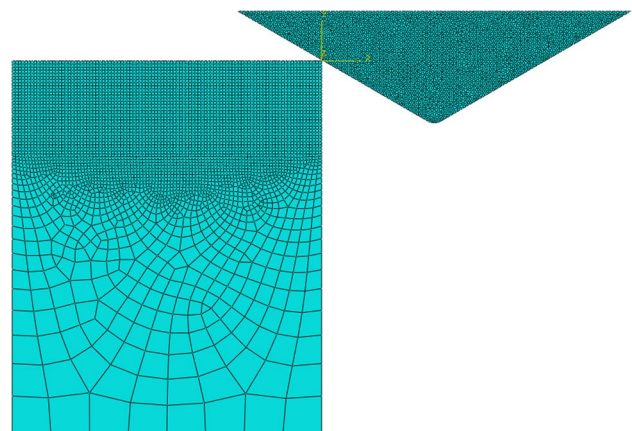


Fig. 3 Geometry model of abrasive particle and workpiece

of the workpiece model were set to $50 \mu\text{m} \times 60 \mu\text{m}$. In order to ensure the accuracy of the calculation results and optimize computational efficiency, a hierarchical grid structure is employed for the workpiece. The upper layer represents the material removal region with refined meshing, while the lower layer serves as the support region with sparse meshing. The four-node plane strain-thermal coupling element with reduction integral is employed as the mesh element type, and the mesh size ranges from 0.5 to 10 μm .

3.2 Material Parameters and Their Corresponding Constitutive Models

Physical property parameters are the characteristics that describe the properties of materials themselves. As shown in Table 1 from literature [16], the material parameters for 20CrMnTi and CBN are listed.

The scratching process is a thermodynamic coupling phenomenon, and the workpiece's specific heat capacity and thermal conductivity exhibit temperature-dependent variations. According to reference [17], Table 2 presents the thermal performance parameters of 20CrMnTi. CBN possesses a specific heat capacity of $430 \text{ J}/(\text{kg}/^\circ\text{C})$ and a thermal conductivity of $80 \text{ W}/\text{m}\cdot^\circ\text{C}$.

Material constitutive model is a mathematical representation of the relationship between stress, strain rate, strain, and temperature of a material. The selection of an appropriate constitutive model is crucial in establishing an accurate simulation model as it directly relates to the properties of the material. The Johnson–Cook model is capable of distinguishing between the processes of strain hardening, strain rate hardening, and heat softening during material deformation, rendering it suitable for a broad range of metallic materials such as steel and aluminum alloys [18]. As 20CrMnTi is classified as a low carbon steel, the Johnson–Cook model has been selected as the constitutive model for this material in this study.

The mathematical expression for the Johnson–Cook model is as follow.

$$\sigma = (A + B \cdot \varepsilon^n) \left(1 + C \cdot \ln \left(\frac{\dot{\varepsilon}}{\dot{\varepsilon}_0} \right) \right) \left(1 - \left(\frac{T - T_0}{T_{melt} - T_0} \right)^m \right) \quad (2)$$

Table 1 Basic physical parameters of CBN and 20CrMnTi

Materials	Density ρ (kg/mm^3)	Elasticity modulus E(Gpa)	Poisson's ratio ν
20CrMnTi	7.8×10^{-6}	207	0.25
CBN	3.48×10^{-6}	909	0.12

Table 2 Thermal performance parameters of 20CrMnTi

Temperature T ($^\circ\text{C}$)	Specific heat c ($\text{J}/\text{kg} \cdot ^\circ\text{C}$)	Thermal conductivity λ ($\text{w}/\text{m} \cdot ^\circ\text{C}$)	Coefficient of linear expansion α ($10^{-6} \cdot ^\circ\text{C}^{-1}$)
20	502	34.5	13.9
100	536	33	16.1
200	586	28	16.7
300	695	17.5	16.7

In this equation, A denotes the yield strength of the material, B represents its strain hardening coefficient, n stands for the strain rate hardening index, C denotes the strain rate hardening coefficient, m represents the thermal softening index, σ signifies the equivalent flow stress of the material, ε indicates equivalent plastic strain, $\dot{\varepsilon}$ represents equivalent plastic strain rate, $\dot{\varepsilon}_0$ represents the equivalent plastic reference strain rate, which is typically assumed to be 1. T represents the current temperature of the material, while T_{melt} denotes its melting point, which is $1440 \text{ }^\circ\text{C}$ for 20CrMnTi. T_0 refers to the ambient temperature at the current atmospheric pressure. The constitutive parameters of 20CrMnTi are presented in Table 3 as per the literature [16].

The wear behavior of particles needs to be observed in the simulation process, so a mathematical expression should be established to describe it accurately. CBN is a brittle material, and its failure behavior mainly occurs when the material deformation exceeds the limit under high stress and fractures. A brittle model can be used to describe the particles of CBN. The ultimate stress for brittle fracture of CBN is 2340 MPa , with an elongation at break of 0.0001 [13].

3.3 Models for Material Failure and Grain-Workpiece Friction

(1) Material failure model

The material failure model serves as a mathematical representation of the formation and continuous removal of debris from the workpiece, which is implemented in finite element software through the elimination of material units. In this study, we have adopted the Johnson–Cook shear damage criterion as our failure criterion for workpiece materials, with its corresponding mathematical expression provided by [18]

Table 3 Constitutive parameters of 20CrMnTi

A (MPa)	B (MPa)	n	C	m
303	192	0.06	0.31	0.706

Table 4 Damage parameters of 20CrMnTi

Parameter	d_1	d_2	d_3	d_4	d_5
Value	-0.77	1.45	-0.47	0.014	3.87

$$D = \sum \frac{\Delta \varepsilon_p}{\varepsilon_f} \quad (3)$$

where D represents the material's failure parameter. When D exceeds 1, the material starts to fail, indicating that the workpiece element is about to be deleted. $\Delta \varepsilon_p$ denotes the equivalent plastic strain increment.

ε_f represents the critical equivalent plastic strain at the time of material failure, which can be calculated as follows:

$$\varepsilon_f = \left(d_1 + d_2 \cdot e^{\frac{d_3 \cdot \varepsilon}{\sigma}} \right) \left(1 + d_4 \cdot \ln \left(\frac{\dot{\varepsilon}_p}{\dot{\varepsilon}_0} \right) \right) \left(1 + d_5 \cdot \left(\frac{T - T_0}{T_{melt} - T_0} \right) \right) \quad (4)$$

where d_1, d_2, d_3, d_4 and d_5 are material damage parameters, and their values are shown in Table 4 [16].

(2) Grain-workpiece friction model

Friction between abrasive particles and workpieces is a significant factor that influences both the magnitude of friction force and the resulting friction temperature. Currently, the prevailing model employed to describe this phenomenon is the Coulomb friction model, which can be mathematically expressed as follows.

$$\begin{cases} \tau_f = \mu \sigma_n & (\mu \sigma_n < \tau_s) \\ \tau_f = \tau_s & (\mu \sigma_n \geq \tau_s) \end{cases} \quad (5)$$

where τ_f represents friction stress, σ_n represents the normal stress at the contact point between the abrasive particle and the workpiece surface, μ represents friction factor. τ_s represents the shear strength of the workpiece.

3.4 Boundary Conditions and Simulation Parameters

During the grinding process, there exists a significantly large ratio between the grinding speed and workpiece feed speed. For a brief period of time, the workpiece can be considered immobile while abrasive particles traverse its surface at the grinding speed. Consequently, in simulations, movement of the workpiece can be restricted by symmetric fixed constraints applied to its bottom node and nodes on both sides of the unrubbed area along horizontal and vertical directions as well as rotational motion in a horizontal plane. The horizontal velocity of the abrasive node should correspond to that of the linear speed of the grinding wheel, with scratch depth

being determined by maximum undeformed chip thickness during grinding.

The grinding speed and maximum undeformed chip thickness are two crucial process parameters that impact the wear condition of abrasive particles. Maximum undeformed chip thickness refers to the deepest point a single abrasive particle can reach into the workpiece, which significantly influences the force exerted by the abrasive particle and leads to different wear forms under various grinding conditions. Grinding speed is a critical factor in determining both sliding speed between abrasive particles and their contact with the front tool surface, as well as affecting friction force between abrasive particles and workpiece. In addition to grinding parameters, characteristics of abrasive particles themselves also affect their wear state. The rake angle of an abrasive particle determines its flow direction, resulting in changes in stress distribution between it and the workpiece. Selecting appropriate grinding parameters and shaping abrasive particles can effectively slow down abrasion processes. This paper mainly conducts finite element simulation of an abrasive wear state based on grinding speed, maximum undeformed chip thickness, and rake angle of abrasives. Specific simulation parameters are shown in Table 5.

MATLAB software was utilized to binarize the images of abrasive particles before and after scratching, enabling the calculation of respective areas A and A' for these particles. Subsequently, the percentage of abrasive wear area $a\%$ which is employed as a crucial criterion for defining the wear patterns of abrasive particles was determined using the following equation.

$$a\% = \frac{A - A'}{A} \times 100\% \quad (6)$$

4 Experimental Verification and Results Discussion

4.1 Experimental Procedure

To understand the specific morphology of CBN particles after wear, a single CBN particle scratching experiment was conducted. Three 40# CBN abrasive grains were selected and scratched under three different maximum

Table 5 Single abrasive scratch simulation parameters

Parameter	Grinding speed v_s (m/s)	Maximum undeformed chip thickness a_{gmax} (μm)	Rake angle of abrasive γ
Value	10,15,20	5,7.5,10	$-60^\circ, -40^\circ, -20^\circ$

undeformed chip thickness experimental conditions using a single abrasive wheel disc prepared in advance on the KVC 800/1 three-axis vertical machining center. The CBN abrasive grains were connected to the matrix of the grinding wheel disc by light-curing resin, and the workpiece used for scratching was 20CrMnTi with a surface roughness less than $0.1\ \mu\text{m}$ after polishing. Friction force is an important index for evaluating grinding performance and sharpness of abrasive particles, and changes in friction force can reflect the process of abrasive wear. During the experiment, Kistler 9257B dynamometer was used to record scratching force at a sampling frequency of 1000HZ, which was then processed using Dynaware software. Figure 4 shows equipment used during this experiment.

When conducting scratching experiments using a single abrasive wheel disc, as illustrated in Fig. 4, the maximum undeformed chip thickness of the abrasive grain $a_{g\max}$ can be determined by Eq. (7) [15]

$$a_{g\max} = 2\pi D \frac{v_w}{v_s} \sqrt{\frac{a_p}{D}} \quad (7)$$

where D represents the diameter of the abrasive particle circulating around the center of the grinding wheel, a_p denotes the grinding depth, v_w indicates the feed speed, and v_s signifies the linear speed of the abrasive particle rotating around the center of the grinding wheel. By varying the feed speed of the table under constant grinding depth and linear speed of abrasive rotation, different maximum undeformed chip thicknesses can be achieved. The scratching experiment is primarily conducted at maximum undeformed chip thicknesses of $5\ \mu\text{m}$, $7.5\ \mu\text{m}$, and $10\ \mu\text{m}$. The experimental parameters are presented in Table 6.

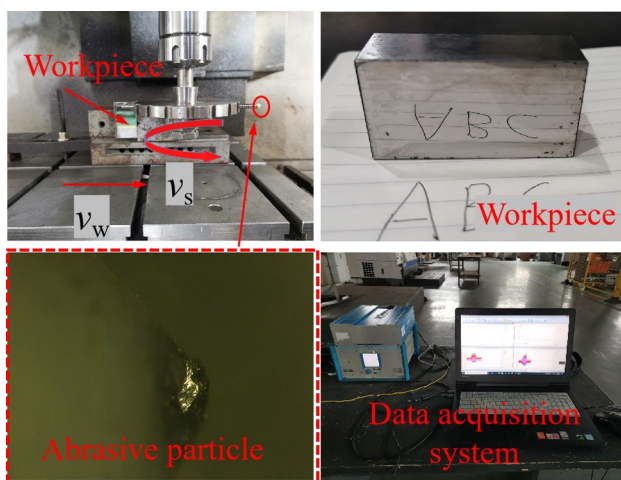


Fig. 4 Experimental setup

Table 6 Experimental parameters

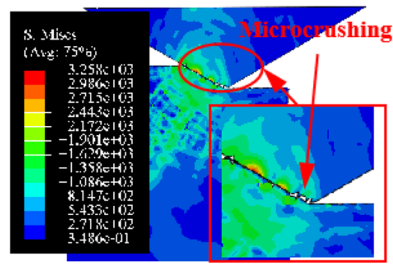
Parameter	Grinding depth a_p (μm)	Linear speed v_s (m/s)	Diameter D (mm)	Feed speed v_w (mm/min)
Value	20	10	120	308, 462, 618

4.2 Comparison of Simulation and Experimental Results of Abrasive Wear

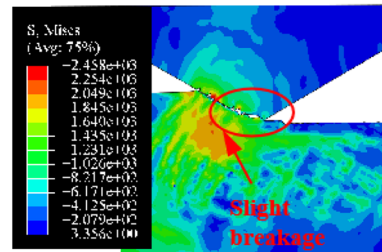
Figure 5a–c illustrate the simulation results of CBN particle with a rake angle of -60° scratching on a 20CrMnTi workpiece at a grinding speed of 10 m/s and maximum undeformed chip thickness set at $5\ \mu\text{m}$. Figure 5d, e respectively present the simulated and measured morphologies of abrasive wear under the same grinding parameters. According to the simulation results, when the abrasive particle traverses 1/3 of the workpiece length, microcrushing occurs at the tip of the abrasive, resulting in a minor removal of CBN material and inducing significant stress on the cutting surface of the abrasive particle. As the abrasive particle traverses 2/3 of the workpiece length, the fractured area of its tip extends towards the front cutter face, resulting in a micro-section formation at the abrasive tip and slight breakage on its front cutter face. As the abrasive particle cuts out the workpiece, the cross section of its tip continuously expands due to friction with the workpiece surface. Simultaneously, the cutting surface of the abrasive particle also experiences small-scale breakage. The scratching experiment, as depicted in Fig. 5e, produced results that were consistent with the simulation. Subsequent to the experiment, abrasive particles exhibited varying degrees of breakage at their tips and a limited range of fractures occurred on the front surface of the tool.

Figure 6a–c illustrate the simulation results of CBN particle with a rake angle of -60° scratching on a 20CrMnTi workpiece at a grinding speed of 10 m/s and maximum undeformed chip thickness set at $7.5\ \mu\text{m}$. Figure 6d, e respectively present the simulated and measured morphologies of abrasive wear under the same grinding parameters. The simulation results indicate that when the abrasive particles traverse 1/3 of the workpiece length, both the abrasive tip and the front cutter face experience varying degrees of breakage, while the overall amount of removed abrasive material is relatively small. When the abrasive particle traverses 2/3 of the workpiece length, a fracture surface is formed between the abrasive tip and the front tool surface due to material removal. As the abrasive particle cuts out the workpiece, the cross section between the front tool face and the tip of the abrasive particle starts to expand inward, leading to crescent-shaped wear on the front tool face. The wear condition of abrasive particle is primarily characterized by fracture, as evidenced in Fig. 5e. The front tool face of

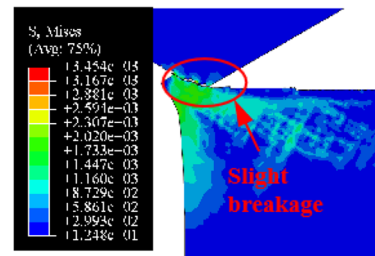
Fig. 5 Simulation and experimental results when the maximum undeformed chip thickness is $5\ \mu\text{m}$



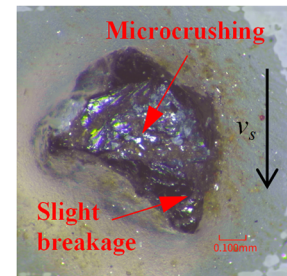
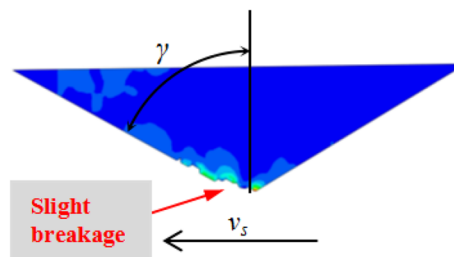
(a) Traverses 1/3 of the workpiece length ($a\%=1.5\%$)



(b) Traverses 2/3 of the workpiece length ($a\%=2.7\%$)



(c) Cut out of the workpiece ($a\%=3.4\%$)



(d) Simulated morphology of abrasive wear (e) Measured morphology of abrasive wear

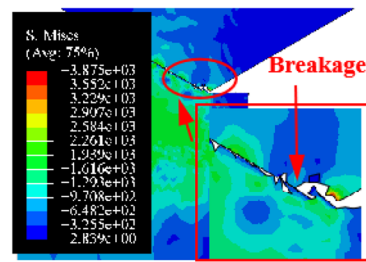
the abrasive particle exhibits a more severe degree of fracture, while only a minor amount of breakage occurs on its flank face when the maximum undeformed chip thickness is $7.5\ \mu\text{m}$.

Figure 7a–c illustrate the simulation results of CBN particle with a rake angle of -60° scratching on a 20CrMnTi workpiece at a grinding speed of 10 m/s and maximum undeformed chip thickness set at $10\ \mu\text{m}$. Figure 7d, e respectively present the simulated and measured morphologies of abrasive wear under the same grinding parameters. It can be seen that the wear pattern of abrasive particle undergoes a gradual

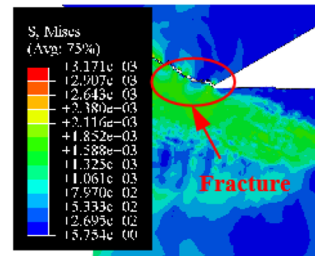
transition from breakage at the front tool face to small-scale fracture at the tip as scratching distance increases, ultimately resulting in the formation of a large crescent-shaped area on the front tool face. The result of scratch test indicates that when the maximum thickness of undeformed chip is $10\ \mu\text{m}$, a significant removal of the material from the front tool face of the abrasive particle occurs, resulting in a loss of grinding ability.

By comparing the results presented in Figs. 5, 6 and 7, it is apparent that when the maximum undeformed chip thickness is small, abrasive wear predominantly occurs at

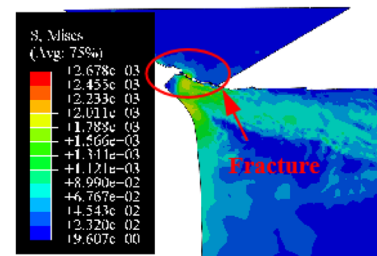
Fig. 6 Simulation and experimental results when the maximum undeformed chip thickness is 7.5 μm



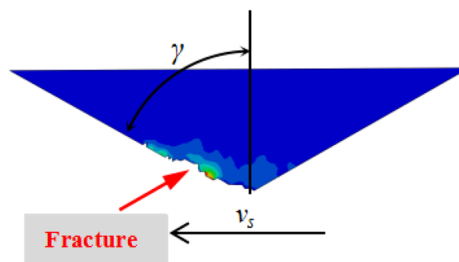
(a) T raverses 1/3 of the workpiece length($\alpha\%=6.5\%$)



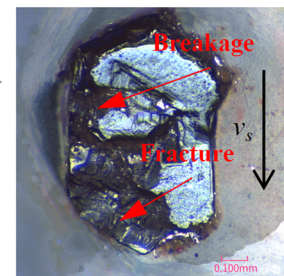
(b) Traverses 2/3 of the workpiece length($\alpha\%=10.5\%$)



(c) Cut out of the workpiece($\alpha\%=11.2\%$)



(d) Simulated morphology of abrasive wear



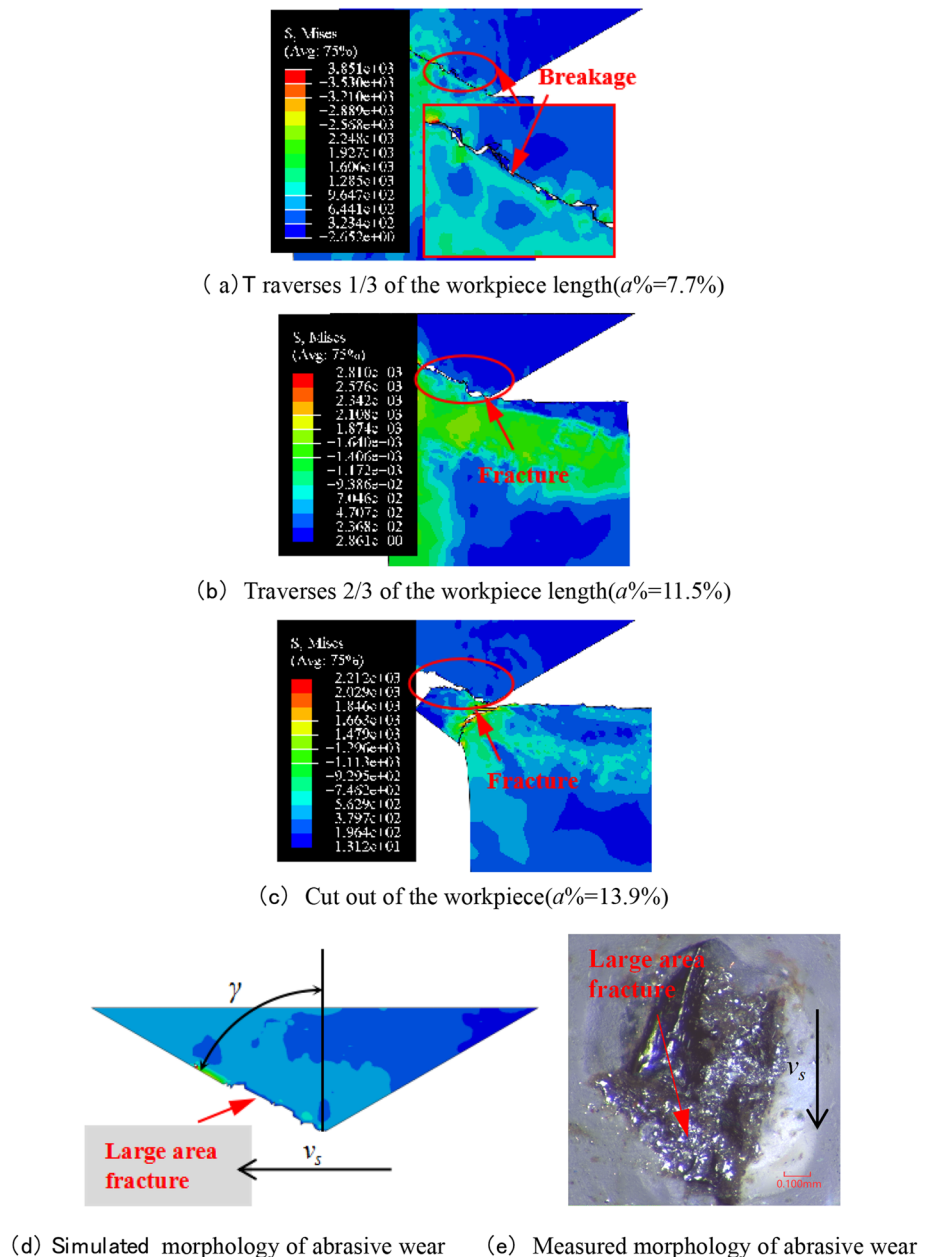
(e) Measured morphology of abrasive wear

the tip of the abrasive with relatively minor damage to the front tool face. An increase in the maximum undeformed chip thickness leads to a gradual escalation in both the magnitude of damage and area affected by abrasive particles. This is due to the inherent brittleness of CBN, which causes it to fracture when surface stress exceeds its limit. As the abrasive particle breaks, the contact area with the workpiece dynamically changes, leading to higher stress concentrations at smaller contact areas and resulting in wear propagation into the interior of the abrasive particle.

4.3 Comparison Between Simulated and Experimental Results of Scratching Force

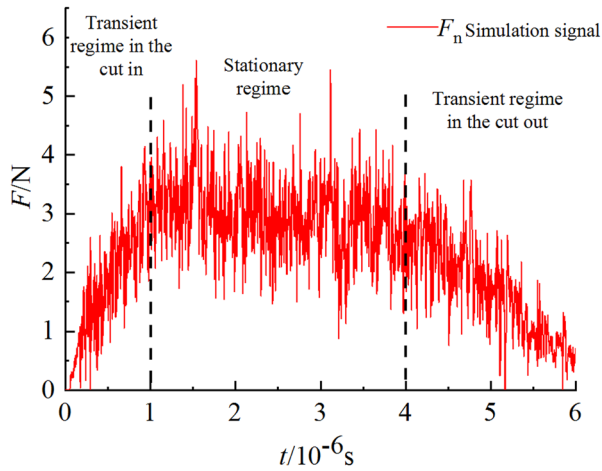
Figure 8 illustrates the simulation and experimental signals of normal scratching force with a maximum undeformed chip thickness of 5 μm . The normal scratching force is a signal characterized by constant fluctuations, as depicted in Fig. 8a. As the abrasive particle cuts into the workpiece, the contact area between them increases continuously, leading to a gradual increase in normal

Fig. 7 Simulation and experimental results when the maximum undeformed chip thickness is $10\ \mu\text{m}$

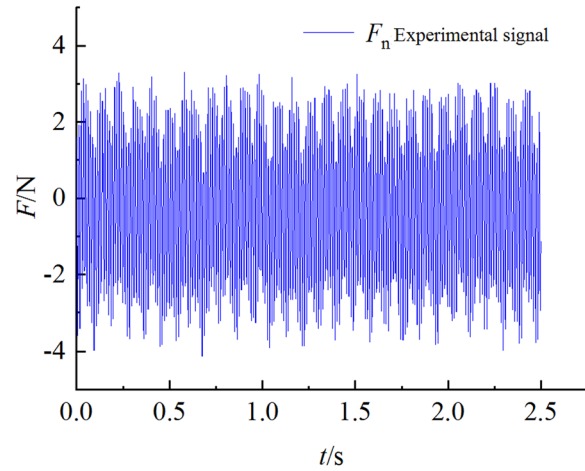


scratching force. Once complete contact is achieved, the normal friction force stabilizes while stress on the abrasive particle continues to rise. If this stress exceeds its ultimate strength, micro-cracks will form and eventually lead to micro-crushing. This causes fluctuations in normal grinding force due to changes in contact area between the abrasive particle and workpiece. During the scratch-out process, material is constantly removed from the workpiece until it can no longer withstand extrusion from abrasive particle and undergoes plastic deformation resulting in a decrease of normal scratching force. Meanwhile, both tip of abrasive particle and front tool face continue breaking off causing small amplitude shocks during reduction of

normal scratching force. The scratching force signal was analyzed within the time range of 1×10^{-6} s to 4×10^{-6} s. During this period, there is no significant change observed in the scratching force, indicating a stable stage of scratching. The average scratching force during this interval is determined as the normal scratching force when the maximum undeformed chip thickness reached $5\ \mu\text{m}$, which amounted to 2.98N. The experimental signal of the normal scratching force within 2.5 s is depicted in Fig. 8b. Due to the inherent vibration of both the tool and workbench during the experiment, as well as the periodic nature of the scratch process, symmetrical periodic variations are observed in the experimental signal. The peak value of



(a) Simulation signal of normal scratching force



(b) Experimental signal of normal scratching force

Fig. 8 Simulation signal and experimental signal of normal scratching force when the maximum undeformed chip thickness is 5 μm

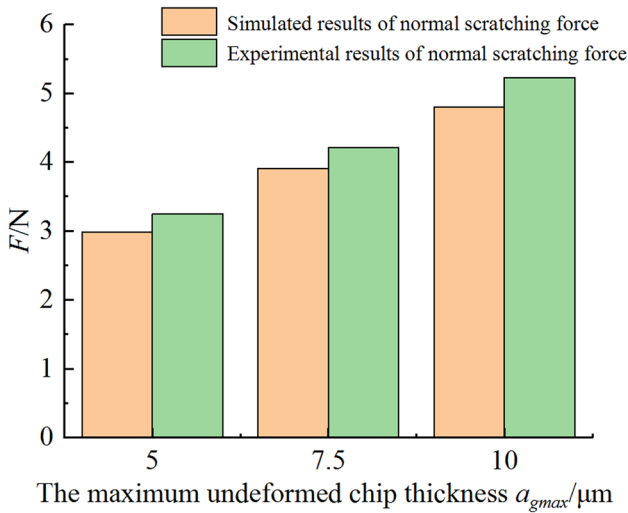


Fig. 9 Comparison between simulated and experimental results of normal scratching force

these periodic changes is considered as the normal scratching force measurement, which amounts to 3.25N.

The results of normal scratching force for maximum undeformed chip thicknesses of 5 μm, 7.5 μm, and 10 μm are presented in Fig. 9. As the maximum undeformed chip thickness increases, both simulated and experimental values of normal scratching force increase. The relative errors between the simulated and calculated normal scratching forces under the aforementioned three maximum undeformed chip thicknesses are 9%, 7.6%, and 8.9% respectively, thereby affirming the reliability of the simulation results in this particular case.

5 Analysis of Simulation Results Under Varying Scratching Speeds and Abrasive Rake Angles

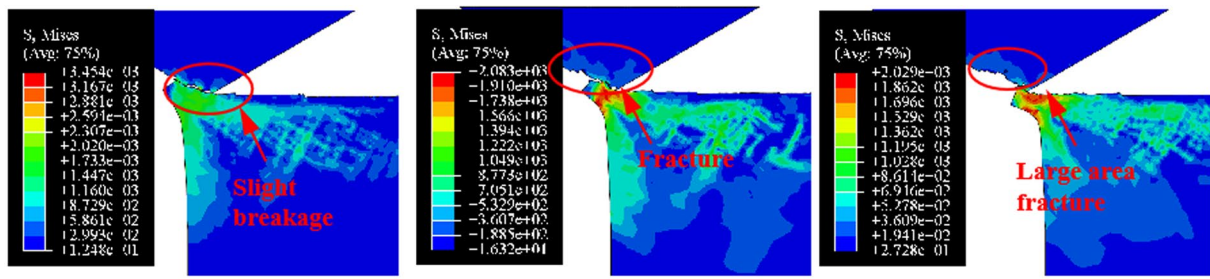
5.1 Impact of Scratching Speed

Figure 10 illustrates the wear characteristics of abrasive particles at different scratching speeds. It can be seen that the exacerbation of CBN wear is observed with an increase in scratching speed. The reason for this is that an increase in scratching speed leads to a faster sliding speed of abrasive chips relative to the front tool face of the abrasive particle, which makes it difficult for the chips to discharge under a large negative rake angle. As a result, they accumulate between the front tool face and workpiece, leading to increased friction and compressive stress on the abrasive particle. When an abrasive particle breaks or fractures, stress in this area increases sharply, making them more susceptible to wear at high scratching speeds.

Figure 11 illustrates the scratching force variation under different scratching speeds. As the grinding speed increases, the normal scratching force gradually decreases due to elevated temperature during the scratching process. The high temperature causes thermal softening of the workpiece material, reducing resistance to grinding debris flow. However, this reduction in normal scratching force is limited by abrasive wear aggravation caused by increased scratching speed.

5.2 Impact of Abrasive Particle Rake Angle

Figure 12 illustrates the wear characteristics of abrasive particles at different rake angle. It is evident that an increase in the abrasive rake angle results in a reduction of CBN



(a) Scratching speed is 10m/s($a\%=3.4\%$) (b) Scratching speed is 15m/s($a\%=11.5\%$) (c) Scratching speed is 20m/s($a\%=18\%$)

Fig. 10 Abrasive wear under various scratching speeds

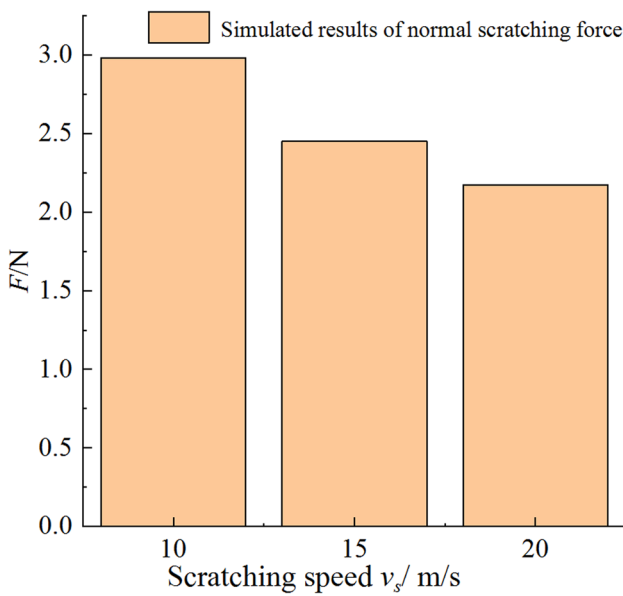


Fig. 11 Scratching force under various scratching speeds

abrasive particle wear. The reason for this is that an increase in the rake angle of abrasive particles facilitates their flow, reduces compressive stress, and consequently slows down the process of abrasive wear.

Figure 13 illustrates the scratching force variation under different abrasive rake angles. The normal scratching force decreases with an increase in the rake angle of the abrasive particle, as this change slows down abrasive wear and ensures a consistently sharp state. Moreover, an increased rake angle also reduces the resultant force during normal decomposition.

6 Conclusion

In order to address the issue of non-uniform wear caused by the structure of the grinding wheel, a two-dimensional finite element simulation model for single abrasive scratching was developed using Abaqus. This model was then combined with an experimental study on single abrasive scratching to analyze the evolution of abrasive wear during the grinding process. The effects of different scratching speeds and abrasive rake angles were examined in terms of their impact on both wear degree and scratching force. Based on these investigations, several conclusions can be drawn.

1. The wear of CBN particles during grinding mainly results from fracture and breakage due to their brittleness.

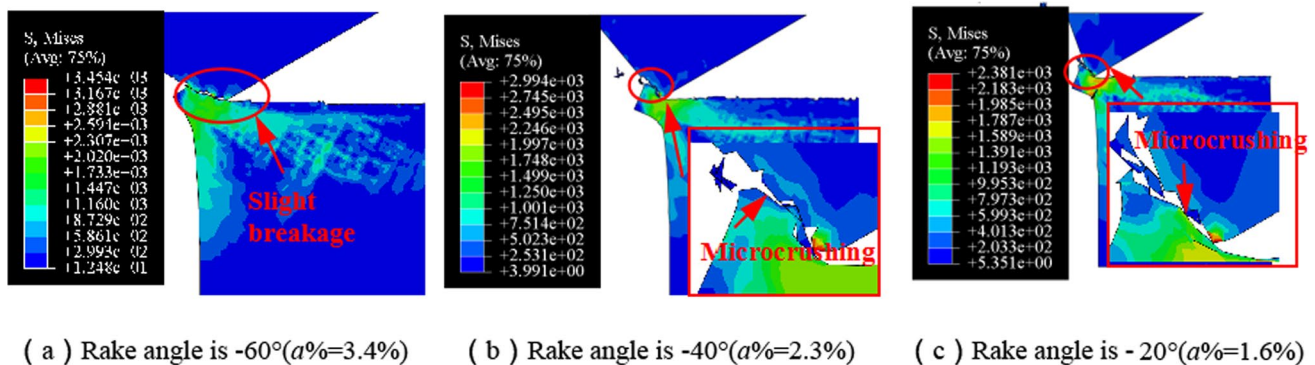


Fig. 12 Abrasive wear under various rake angles

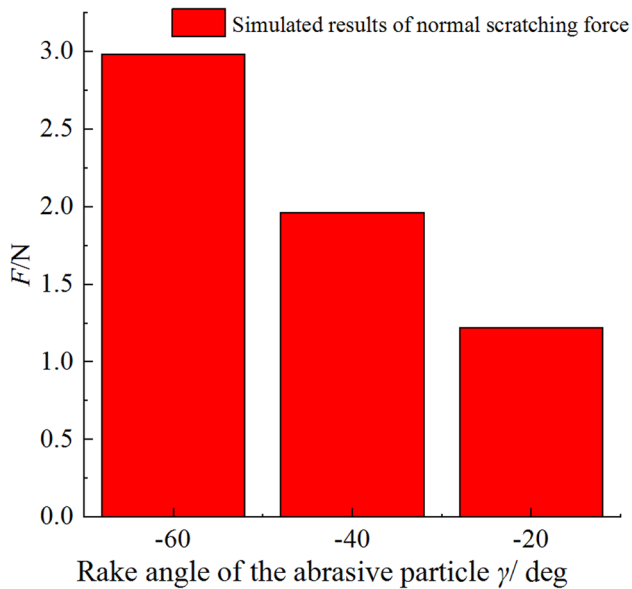


Fig. 13 Scratching force under various abrasive rake angles

- In the case of a constant scratching speed and abrasive rake angle, an increase in the maximum undeformed chip thickness (i.e., an increase in the intermittent ratio of the grinding wheel) results in elevated abrasive wear and concurrently leads to heightened scratching force. In severe cases, this can cause extensive fracture areas on the abrasive, leading to a loss of its grinding effectiveness.
- As the scratching speed increases, more chips will accumulate in the position of the front tool face of the abrasive particles when they scratch the workpiece with a large negative rake angle, resulting in an increase in the wear degree of the abrasive particles. However, this increase in scratching speed also elevates the temperature between the abrasive particles and workpiece, resulting in partial softening of the workpiece and subsequently reducing the scratching force.
- With an increase in the rake angle of the abrasive particles, chips can flow more efficiently along the front tool face towards the external environment, thereby reducing compressive stress and friction resulting from chip accumulation and decelerating wear on the front tool face of the abrasive particles.

Acknowledgements The authors gratefully acknowledge the financial support for this work by the Hunan Youth Science and Technology Innovation Talents Project (Grant No. 2023RC3178) and National Natural Science Foundation of China (Grant No. 51905168).

Author Contributions YJ: Conceptualization, methodology, investigation, formal analysis, validation, resources, writing—original draft. WZ: Conceptualization, methodology, investigation, writing—original

draft, software. YT: Investigation, software, validation. DH: Supervision, validation. ZW: Supervision, validation.

Declarations

Competing interests The authors declare that they have no competing interests.

References

- Li, C., Shi, Z. J., Zhang, X. H., et al. (2020). An investigation on grinding mechanism of alumina ceramic using a grooved grinding wheel with inclined cross section. *The International Journal of Advanced Manufacturing Technology*, 111, 2391–2399.
- Maeng, S., Ito, H., Kakinuma, Y., et al. (2023). Study on cutting force and tool wear in machining of die materials with textured PCD tools under ultrasonic elliptical vibration. *International Journal of Precision Engineering and Manufacturing-Green Technology*, 10(1), 35–44.
- Wei, S., Zhang, T., Wei, H., et al. (2023). Simulation study on removal mechanism of Si_3N_4 ceramic in rotary ultrasonic grinding. *International Journal of Precision Engineering and Manufacturing*, 24(6), 945–965.
- Jackson, M. J. (2007). Modelling of fracture wear in vitrified CBN grinding wheels. *Surfaces*, 6, 10.
- Su Chong, Xu., Li, L. Y., et al. (2013). Numerical simulation of cutting process of CBN grit based on SPH method. *China Mechanical Engineering*, 24(05), 667–671.
- Zhang, J. Q., Guan, P., Su, C., et al. (2011). Simulation of vitrified CBN grinding wheel abrasive wear based on SPH. *Advanced Materials Research*, 317–319, 498–502.
- Ding, W. F., Miao, Q., Zhu, Y. J., et al. (2016). Comparative investigation on wear behavior and self-sharpening phenomenon of polycrystalline cubic boron nitride and monocrystalline cubic boron nitride grains in high-speed grinding. *Proceedings of the Institution of Mechanical Engineers, Part B: Journal of Engineering Manufacture*, 230(4), 710–721.
- Ding, W. F., Zhu, Y. J., Xu, J. H., et al. (2015). Finite element investigation on the evolution of wear and stresses in brazed CBN grits during grinding. *The International Journal of Advanced Manufacturing Technology*, 81(5), 985–993.
- Mei, Y. M., Yu, Z. H., & Yang, Z. S. (2017). Numerical investigation of the evolution of grit fracture and its impact on cutting performance in single grit grinding. *The International Journal of Advanced Manufacturing Technology*, 89(9), 3271–3284.
- Wang, J. W., Yu, T. Y., Ding, W. F., et al. (2018). Wear evolution and stress distribution of single CBN superabrasive grain in high-speed grinding. *Precision Engineering*, 54, 70–80.
- Rao, Z. W., Ding, W. F., Zhu, Y. J., et al. (2018). Numerical simulation analysis and experimental validation on wear/fracture mechanisms of polycrystalline cubic boron nitride superabrasives in high-speed grinding. *Ceramics International*, 45(3), 3377–3389.
- Wang, J. W., Ding, W. F., Zhu, Y. J., et al. (2019). Micro-fracture variation and grinding performance of PCBN superabrasive grains in high-speed grinding. *International Journal of Mechanical Sciences*, 160, 15–25.
- Bergs, T., Ohlert, M., Prinz, S., et al. (2020). Modeling of the Fracture Behavior of CBN Grains during Single Grain Dressing using FEM. *Procedia CIRP*, 93, 1514–1519.
- Wang, F. W., Chen, Y. L., Gao, Y., et al. (2021). Peridynamic simulation to fracture mechanism of CBN grain in the honing wheel dressing process. *Micromachines*, 12(10), 1186–1206.

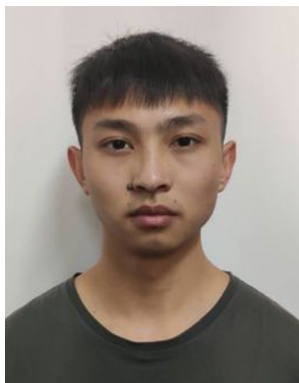
15. Yi, J., Yi, T., Deng, H., et al. (2023). Theoretical modeling and experimental study on grinding force of straight groove structured grinding wheel. *The International Journal of Advanced Manufacturing Technology*, 124(10), 3407–3421.
16. Gao, Y., Wang, F., Liang, Y., et al. (2021). Cutting performance of randomly distributed active abrasive grains in gear honing process. *Micromachines*, 12(9), 1119–1135.
17. Wang, X., Wei, X., Yang, X., et al. (2013). Atomic diffusion of gradient ultrafine structured surface layer produced by T10 steel rubbing against 20CrMnTi steel. *Wear*, 304(1–2), 118–125.
18. Yiming, M. (2017). *Research on grit wear process and monitoring technique of grain wear in single-grit grinding*. Zhejiang University.

Publisher's Note Springer Nature remains neutral with regard to jurisdictional claims in published maps and institutional affiliations.

Springer Nature or its licensor (e.g. a society or other partner) holds exclusive rights to this article under a publishing agreement with the author(s) or other rightsholder(s); author self-archiving of the accepted manuscript version of this article is solely governed by the terms of such publishing agreement and applicable law.



Jun Yi is currently an associate professor in College of Mechanical Engineering, Hunan university of science and technology, China. His research interests focused on the high efficiency and precision machining of difficult-to-cut materials and complex curved parts.



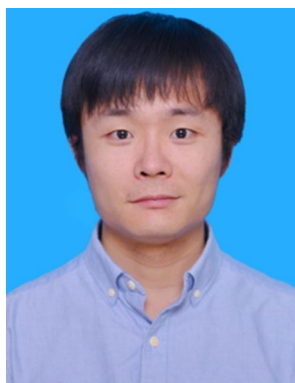
Zongwei Wang is a postgraduate student at the School of Mechanical Engineering, Hunan University of Science and Technology, China. His main research interest is structured grinding wheel light curing rapid prototyping.



Tao Yi received the M.S. from Department of Mechanical Engineering at Hunan University of Science and Technology, China, in 2023. He is currently engaged in precision machining of basic components such as gears and bearings.



Hui Deng is currently a professor in College of Mechanical Engineering, Hunan university of science and technology, China. He is mainly engaged in the research of intelligent manufacturing technology, laser micro-nano processing technology, laser dressing technology, laser micro-structure technology, laser processing monitoring and control technology, difficult-to-cut materials grinding technology, etc.



Wei Zhou received his Ph.D. in Mechanical Engineering from the College of Mechanical and Electrical Engineering, Central South University, China, in 2016. He joined College of Mechanical Engineering, Hunan university of science and technology, China, in 2016. His interest is in gear anti-fatigue design, surface tribology, mechanical parts structural strength design.